EPJ Web of Conferences **137**, 01014 (2017) DOI: 10.1051/epjconf/201713701014
XIIth Quark Confinement & the Hadron Spectrum

Roy–Steiner-equation analysis of pion–nucleon scattering

U.-G. Meißner[1,2,a], J. Ruiz de Elvira[1,3,b], M. Hoferichter[4], and B. Kubis[1]

[1] *Helmholtz-Institut für Strahlen- und Kernphysik (Theorie) and Bethe Center for Theoretical Physics, Universität Bonn, D–53115 Bonn, Germany*
[2] *Institut für Kernphysik, Institute for Advanced Simulation, and Jülich Center for Hadron Physics, Forschungszentrum Jülich, D–52425 Jülich, Germany*
[3] *Albert Einstein Center for Fundamental Physics, Institute for Theoretical Physics, University of Bern, Sidlerstrasse 5, CH–3012 Bern, Switzerland*
[4] *Institute for Nuclear Theory, University of Washington, Seattle, WA 98195-1550, USA*

Abstract. Low-energy pion–nucleon scattering is relevant for many areas in nuclear and hadronic physics, ranging from the scalar couplings of the nucleon to the long-range part of two-pion-exchange potentials and three-nucleon forces in Chiral Effective Field Theory. In this talk, we show how the fruitful combination of dispersion-theoretical methods, in particular in the form of Roy–Steiner equations, with modern high-precision data on hadronic atoms allows one to determine the pion–nucleon scattering amplitudes at low energies with unprecedented accuracy. Special attention will be paid to the extraction of the pion–nucleon σ-term, and we discuss in detail the current tension with recent lattice results, as well as the determination of the low-energy constants of chiral perturbation theory.[c]

1 Introduction

Pion–nucleon scattering is one of the most fundamental processes involving the lightest mesons and baryons, hence allowing one to test, at low energies, the dynamical constraints imposed by chiral symmetry. For instance, its low-energy parameters, especially the scattering lengths, encode crucial information about the spontaneous and explicit breaking of chiral symmetry as realized in the nucleon sector [3, 4]. In particular, at leading order (LO) in the chiral expansion, i.e., in the expansion in pion masses and momenta, the two pion–nucleon scattering lengths are completely determined by a well-known low-energy theorem (LET), which predicts the isospin-odd scattering length in terms of the pion (M_π) and nucleon (m_N) masses as well as the pion decay constant F_π, while the isospin-even one is suppressed.

This expansion around the chiral limit of QCD in terms of momenta and quark masses can be performed systematically in the framework of Chiral Perturbation Theory (ChPT) [5–7]. Nevertheless, at next-to-leading order (NLO), the πN scattering amplitude depends on a list of low-energy constants (LECs), which, encoding information about heavier degrees of freedom, cannot be constrained from

[a] Speaker, e-mail: meissner@hiskp.uni-bonn.de
[b] Speaker, e-mail: elvira@itp.unibe.ch
[c] These proceedings borrow heavily from a previous conference contribution [1], as well as from our original article [2].

chiral symmetry alone. Once determined in one process, these LECs can subsequently be used to predict others. For πN scattering this implies applications that reach far into the domain of nuclear physics, where the same LECs that appear in the πN amplitude govern the long-range part of the nucleon–nucleon (NN) potential and the three-nucleon force.

In addition, also the partial waves for the crossed channel $\pi\pi \to \bar{N}N$ enter applications that extend beyond the πN system. The response of the nucleon to external currents can be analyzed via a t-channel dispersion relation, and depending on the quantum numbers $\pi\pi$ intermediate states frequently provide the dominant contribution to the integral. In particular, for the P-waves, it provides a determination of the $\pi\pi$ continuum contribution to the isovector spectral functions of the nucleon electromagnetic form factors [8], an essential input for the analysis of the proton radius puzzle.

Finally, a further strong incentive to study pion–nucleon scattering derives from its relation to the pion–nucleon σ-term $\sigma_{\pi N}$, defined via the scalar form factor of the nucleon

$$\sigma(t) = \frac{1}{2m_N}\langle N(p')|\hat{m}(\bar{u}u + \bar{d}d)|N(p)\rangle, \qquad \hat{m} = \frac{m_u + m_d}{2}, \qquad \sigma_{\pi N} \equiv \sigma(0), \qquad t = (p' - p)^2. \quad (1)$$

The relation between $\sigma_{\pi N}$ and the πN scattering amplitude proceeds by means of the Cheng–Dashen LET [9, 10], which requires an analytic continuation of the Born-term-subtracted isoscalar amplitude into the unphysical region. The σ-term has gathered strong interest beyond the hadron physics community in recent years, due to its relation to the scalar couplings of the nucleon that are prerequisite for a consistent interpretation of direct-detection dark matter searches [11–13].

2 Roy–Steiner equations for πN scattering

In recent years, it has been repeatedly proven that the combination of ChPT with dispersive techniques can be used to increase the predictive power of chiral symmetry. Dispersion relations exploit analyticity and crossing symmetry to arrive at a representation that relates the amplitude at an arbitrary point in the complex plane to an integral over its imaginary part. Once the amplitude is partial-wave projected, unitarity relates the real and imaginary parts of the amplitude, which leads to a self-consistent system of equations for the partial-wave phase shifts, so-called partial-wave dispersion relations (PWDRs). The subtraction constants, the only free parameters, can frequently be pinned down by matching to ChPT. The dispersive representation thus provides an ideal framework to reliably perform an analytic continuation into the complex plane or into the unphysical region, which for instance becomes central for the extraction of the pion–nucleon σ-term. In particular, for $\pi\pi$ scattering, the use of Roy equations [14] has led to a determination of the low-energy $\pi\pi$ scattering amplitude with unprecedented accuracy [15, 16], which, for the first time, allowed for a precise determination of the $f_0(500)$ pole parameters [17, 18].

In the case of πN scattering, a full system of PWDRs has to include dispersion relations for two distinct physical processes, $\pi N \to \pi N$ (s-channel) and $\pi\pi \to \bar{N}N$ (t-channel), and the use of $s \leftrightarrow t$ crossing symmetry will intertwine s- and t-channel equations. Roy–Steiner (RS) equations [19] are a set of PWDR that combine the s- and t- channel physical region by means of hyperbolic dispersion relations (HDRs). Subtractions are performed at the so-called subthreshold point, which proves convenient for the matching to ChPT and for the extrapolation to the Cheng–Dashen point [9], and thus for establishing the relation to $\sigma_{\pi N}$ by means of the LET [9, 10]. Furthermore, a reliable extrapolation to the subthreshold region requires additional input from the t-channel ($\pi\pi \to \bar{N}N$) partial waves [20–22], a requirement that is straightforward to comply with in the RS formalism, as HDRs by construction intertwine all physical regions. The construction of a complete system of RS equations

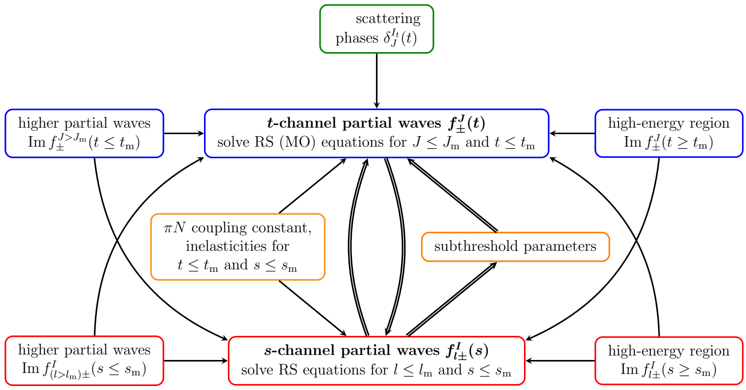

Figure 1. Solution strategy for RS equations in πN scattering. The s- and t-channel partial waves will be solved for up to angular momenta $l_\mathrm{m} = 1$ and $J_\mathrm{m} = 2$, respectively. Figure taken from [2].

for πN scattering has been presented in detail in [2, 23]; see also [24–26] for partial results. For the s-channel partial waves, they read [19]

$$\begin{aligned} f_{l+}^I(W) = N_{l+}^I(W) &+ \frac{1}{\pi}\int\limits_{t_\pi}^{\infty} \mathrm{d}t' \sum_J \Big\{ G_{lJ}(W,t')\, \mathrm{Im}\, f_+^J(t') + H_{lJ}(W,t')\, \mathrm{Im}\, f_-^J(t') \Big\} \\ &+ \frac{1}{\pi}\int\limits_{W_+}^{\infty} \mathrm{d}W' \sum_{l'=0}^{\infty} \Big\{ K_{ll'}^I(W,W')\, \mathrm{Im}\, f_{l'+}^I(W') + K_{ll'}^I(W,-W')\, \mathrm{Im}\, f_{(l'+1)-}^I(W') \Big\}, \end{aligned} \tag{2}$$

where due to G-parity only even/odd J contribute for isospin $I = +/-$, respectively. The kernels $K_{ll'}^I(W,W)$, $G_{lJ}(W,t)$, and $H_{lJ}(W,t)$ are known analytically, and $N_{l+}^I(W)$ denotes the partial-wave projections of the pole terms.

For the t-channel partial-wave projection, the corresponding t-channel RS equations are [23]

$$\begin{aligned} f_+^J(t) = \tilde{N}_+^J(t) &+ \frac{1}{\pi}\int\limits_{t_\pi}^{\infty} \mathrm{d}t' \sum_{J'} \Big\{ \tilde{K}_{JJ'}^1(t,t')\, \mathrm{Im}\, f_+^{J'}(t') + \tilde{K}_{JJ'}^2(t,t')\, \mathrm{Im}\, f_-^{J'}(t') \Big\} \\ &+ \frac{1}{\pi}\int\limits_{W_+}^{\infty} \mathrm{d}W' \sum_{\ell=0}^{\infty} \Big\{ \tilde{G}_{J\ell}(t,W')\, \mathrm{Im}\, f_{\ell+}^I(W') + \tilde{G}_{J\ell}(t,-W')\, \mathrm{Im}\, f_{(\ell+1)-}^I(W') \Big\}, \end{aligned} \tag{3}$$

and similarly for f_-^J except for the fact that these do not receive contributions from f_+^J. In addition, only even or odd J' couple to even or odd J (corresponding to t-channel isospin $I_t = 0$ or $I_t = 1$), respectively, and only higher t-channel partial waves contribute to lower ones.

The strategy for the solution of the RS equations is outlined in Fig. 1: in the s-channel, the six S- and P-waves $f_{l\pm}^I$, with $I = \pm$ for the isospin index and orbital angular momentum l, are considered dynamically below a matching point s_m, whereas the imaginary parts of higher partial waves for all s, the imaginary parts of the S- and P-waves above s_m, and, potentially, inelasticities below s_m are required as input. In practice, the matching point is chosen at its optimal value $s_\mathrm{m} = (1.38\,\mathrm{GeV})^2$ as argued in [23]. In contrast to the six s-channel amplitudes, there are only three S- and P-waves in the t-channel, $f^J_\pm$, with total angular momentum J and the subscript referring to parallel/antiparallel antinucleon–nucleon helicities. Below the first inelastic threshold, the t-channel unitarity relations are linear in $f^J_\pm$

$$\operatorname{Im} f^J_\pm(t) = \sigma^\pi_t \big(t^{I_t}_J(t)\big)^* f^J_\pm(t), \tag{4}$$

from which one can infer Watson's final-state interaction theorem [27], stating that (in the elastic region) the phase of $f^J_\pm$ is given by the phase $\delta^{I_t}_J$ of the respective $\pi\pi$ scattering partial wave $t^{I_t}_J$. It implies that the equations for the t-channel partial waves take the form of a Muskhelishvili–Omnès (MO) problem [28, 29], whose solution requires—in addition to higher partial waves and the imaginary parts above the matching point t_m—input for the $\pi\pi$ phase shifts.

Given that data in the t-channel reaction $\pi\pi \to \bar{N}N$ become available only above the two-nucleon threshold, the solution of the t-channel equations is subject to an additional complication that is related to the large pseudophysical region in this reaction. Thus, the amplitudes in the pseudophysical region $t_\pi \leq t \leq t_N$ required for the t-channel integrals need to be reconstructed from unitarity. While for every partial wave $\pi\pi$ intermediate states generate by far the dominant contribution, intermediate states besides $\pi\pi$ become relevant in the unitarity relation around 1 GeV, most notably in the S-wave, where $\bar{K}K$ intermediate states account for the occurrence of the $f_0(980)$ resonance [30].

Once the t-channel problem is solved, the resulting t-channel partial waves are used as input for the s-channel problem, which then reduces to the form of conventional $\pi\pi$ Roy equations. The basic idea can be summarized in such a way that the phase shifts at low energies, from the πN threshold to s_m, are represented in suitable parameterizations whose free parameters, together with the subtraction constants, are determined by minimizing the difference between the left-hand side (LHS) and right-hand side (RHS) of (2),

$$\Delta^2_\mathrm{RS} = \sum_{l,I_s,\pm} \sum_{j=1}^{N} \left(\frac{\operatorname{Re} f^{I_s}_{l\pm}(W_j) - F\left[f^{I_s}_{l\pm}\right](W_j)}{\operatorname{Re} f^{I_s}_{l\pm}(W_j)} \right)^2 . \tag{5}$$

In addition, we found that the solution can be stabilized substantially when the S-wave scattering lengths, known very precisely from pionic atoms [2, 31, 32], are imposed as constraints

$$a^{1/2}_{0+} = (169.8 \pm 2.0) \times 10^{-3} M_\pi^{-1}, \qquad a^{3/2}_{0+} = (-86.3 \pm 1.8) \times 10^{-3} M_\pi^{-1}. \tag{6}$$

Eventually, a full solution of the system can be obtained by iterating this procedure until all partial waves and parameters are determined self-consistently. In practice, virtually all interdependence proceeds via the subtractions constants, so that the need for an iterative procedure can be avoided if the corresponding terms are included explicitly in the s-channel fit. In this way, the minimization of (5) provides us with a new set of subthreshold parameters and S- and P-wave phase shifts, which, at the same time, satisfy both the s-channel (2) and t-channel (3) RS equations.

A full error analysis of the RS solutions was performed in [2] and includes the following number of effects: first, the input for the matching conditions as well as for the energy region above the matching point and higher partial waves is varied, both regarding different partial-wave analyses [33–36] and truncations of the partial-wave expansion. Furthermore, the πN coupling constant $g^2/(4\pi) = 13.7(2)$ [31, 32] is also varied within uncertainties and the sensitivity to the parameterization of the low-energy phase shifts used in the solution is investigated. Second, it is also observed that the RS equations are more sensitive to some subthreshold parameters than others. To account for this effect, a set of solutions corresponding to different starting values of the χ^2-minimization are generated, while imposing sum rules for the higher subthreshold parameters, and the observed distribution is taken as

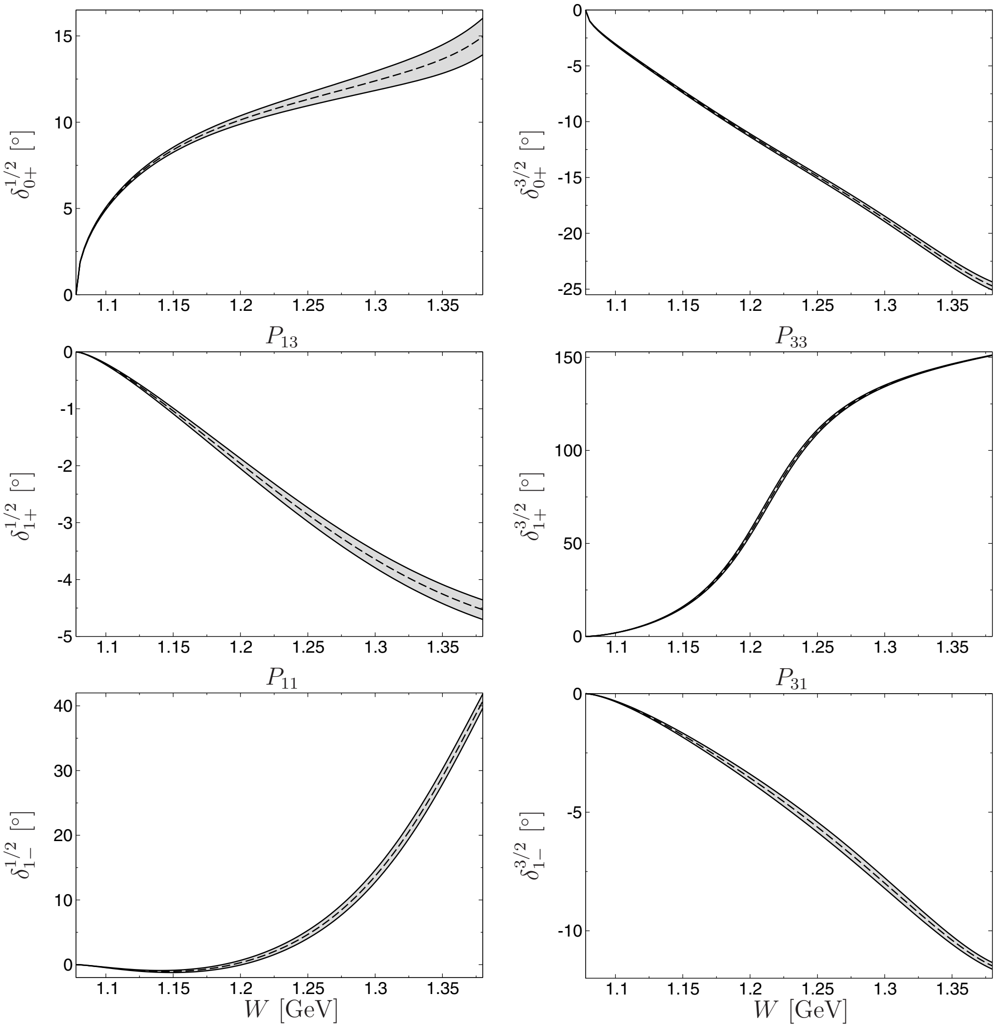

Figure 2. Error bands for the πN phase shifts. The dashed lines indicate the central curves. Figure taken from [2].

an additional source of uncertainty. Third, the errors in the scattering lengths are propagated, which crucially enter as constraints in the minimization, to the results for the subthreshold parameters.

The corresponding results for the *s*-channel partial-wave phase shifts are plotted in Fig. 2 while the solutions for the *t*-channel are shown in [2]. The resulting subthreshold parameters are given in Table 1, compared to the KH80 values [33, 34]. We also keep track of the correlations between subthreshold parameters, obtaining a 13×13 covariance matrix that encodes uncertainties and correlations of the 13 subthreshold parameters, which will be relevant for the matching to ChPT.

Table 1. Subthreshold parameters from the RS analysis in comparison with the KH80 values [33, 34]. Table taken from [2].

	RS	KH80
d^+_{00} [M_π^{-1}]	-1.361 ± 0.032	-1.46 ± 0.10
d^+_{10} [M_π^{-3}]	1.156 ± 0.019	1.12 ± 0.02
d^+_{01} [M_π^{-3}]	1.155 ± 0.016	1.14 ± 0.02
d^+_{20} [M_π^{-5}]	0.196 ± 0.003	0.200 ± 0.005
d^+_{11} [M_π^{-5}]	0.185 ± 0.003	0.17 ± 0.01
d^+_{02} [M_π^{-5}]	0.0336 ± 0.0006	0.036 ± 0.003
d^-_{00} [M_π^{-2}]	1.411 ± 0.015	1.53 ± 0.02
d^-_{10} [M_π^{-4}]	-0.159 ± 0.004	-0.167 ± 0.005
d^-_{01} [M_π^{-4}]	-0.141 ± 0.005	-0.134 ± 0.005
b^+_{00} [M_π^{-3}]	-3.455 ± 0.072	-3.54 ± 0.06
b^-_{00} [M_π^{-2}]	10.49 ± 0.11	10.36 ± 0.10
b^-_{10} [M_π^{-4}]	1.000 ± 0.029	1.08 ± 0.05
b^-_{01} [M_π^{-4}]	0.208 ± 0.020	0.24 ± 0.01

3 Consequences for the πN σ-term

The Cheng–Dashen LET [9, 10] relates the Born-term-subtracted isoscalar amplitude evaluated at the Cheng–Dashen point ($\nu = 0, t = 2M_\pi^2$) to the scalar form factor of the nucleon, evaluated at momentum transfer $t = (p' - p)^2 = 2M_\pi^2$,

$$\bar{D}^+(0, 2M_\pi^2) = \sigma(2M_\pi^2) + \Delta_R, \tag{7}$$

where Δ_R represents higher-order corrections in the chiral expansion, which are expected to be small. Here, we use the estimate $|\Delta_R| \lesssim 2\,\text{MeV}$ [37], derived from resonance saturation for the $O(p^4)$ LECs. In practice, the relation (7) is often rewritten as

$$\sigma_{\pi N} = \sigma(0) = \Sigma_d + \Delta_D - \Delta_\sigma - \Delta_R, \tag{8}$$

where $\Delta_\sigma = \sigma(2M_\pi^2) - \sigma_{\pi N}$ measures the curvature in the scalar form factor, $\Delta_D = \bar{D}^+(0, 2M_\pi^2) - \Sigma_d$ parameterizes contributions to the πN amplitude beyond the first two terms in the subthreshold expansion, and $\Sigma_d = F_\pi^2(d^+_{00} + 2M_\pi^2 d^+_{01})$. As shown in [38], although these corrections are large individually due to strong rescattering in the isospin-0 $\pi\pi$ S-wave, they cancel to a large extent in the difference. For the numerical analysis we use $\Delta_D - \Delta_\sigma = (-1.8 \pm 0.2)\,\text{MeV}$ [30, 39]. Finally, the RS results for the subthreshold parameters d^+_{00} and d^+_{01} in Table 1 give $\Sigma_d = (57.9 \pm 1.9)\,\text{MeV}$, which based on (8) translates immediately to [40]

$$\sigma_{\pi N} = (59.1 \pm 3.5)\,\text{MeV}, \tag{9}$$

which already includes isospin-breaking corrections in the LET [41–43].

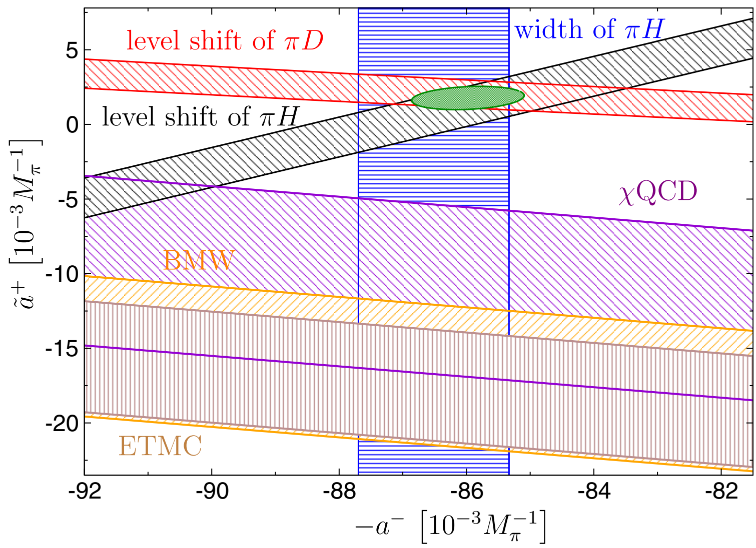

Figure 3. Constraints on the πN scattering lengths from pionic atoms and lattice σ-terms. Figure taken from [49].

This result implies a significant increase compared to the "canonical value" of $\sigma_{\pi N} \sim 45\,\text{MeV}$ [44], although already 4.2 MeV are due to new corrections to the LET. The remaining increase of nearly 10 MeV is dictated by the new scattering length values from pionic-atom experiments. To illustrate the dependence of the σ-term on the scattering lengths used as input to the solution, we expand Σ_d linearly around the central values and find

$$\Sigma_d = (57.9 \pm 0.9)\,\text{MeV} + \sum_{I_s} c_{I_s} \Delta a_{0+}^{I_s}, \qquad c_{1/2} = 0.24\,\text{MeV}, \qquad c_{3/2} = 0.89\,\text{MeV}, \tag{10}$$

where $\Delta a_{0+}^{I_s}$ gives the deviation from the scattering lengths extracted from hadronic atoms in units of $10^{-3}M_\pi^{-1}$. This linearized version produces $\Sigma_d = (46 \pm 4)\,\text{MeV}$ if the KH80 scattering lengths are used, in excellent agreement with the original KH80 value $\Sigma_d = (50 \pm 7)\,\text{MeV}$. Nevertheless, our result for the σ-term seems to be somewhat at odds with a series of recent lattice $\sigma_{\pi N}$ calculations performed near or at physical pion masses, which yield values

$$\begin{aligned} &\sigma_{\pi N} = 38(3)(3)\,\text{MeV} && \text{(BMW [45])}, && \sigma_{\pi N} = 44.4(3.2)(4.5)\,\text{MeV} && (\chi\text{QCD [46]}),\\ &\sigma_{\pi N} = 37.2(2.6)(^{+1.0}_{-0.6})\,\text{MeV} && \text{(ETMC [47])}, && \sigma_{\pi N} = 35.0(6.1)\,\text{MeV} && \text{(RQCD [48])}. \end{aligned} \tag{11}$$

Such smaller values are indeed more consistent with analyses of flavor SU(3) breaking in the baryon spectrum and the OZI rule for scalar strangeness matrix elements of the nucleon. However, these lattice results are in significant tension with the pionic-atom spectroscopy measurements [50–52]: the linear relation between $\sigma_{\pi N}$ and the πN scattering lengths in (10) can be inverted so that a given value for the σ-term imposes a constraint in the scattering-length plane [49]. The constraints corresponding to the lattice results of [45–47] compared to the bands extracted from pionic atoms are shown in Fig. 3, which reflects the core of the discrepancy between lattice and phenomenology: while the three bands from the pionic-atom measurements nicely overlap, the lattice σ-terms favor a considerably smaller value of $\tilde{a}^+$ [49]. A lattice calculation of the πN scattering lengths may be a good way to illuminate the cause of this discrepancy.

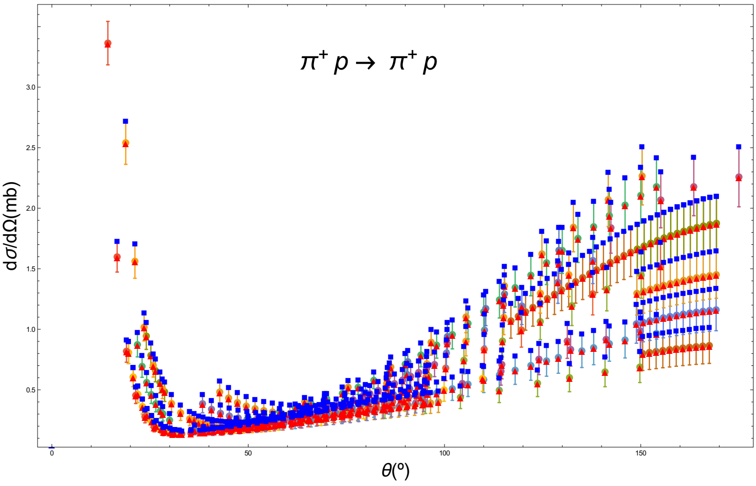

Figure 4. $\pi^+ p \to \pi^+ p$ differential cross section as a function of the scattering angle θ for $T_\pi \leq 50\,\text{MeV}$. The experimental data are taken from the GWU-SAID data base [36], with each experiment denoted by a differently colored error bar. Red triangles and blue squares correspond to the RS solution generated with scattering lengths extracted from pionic atoms and KH80, respectively.

Nonetheless, an additional way to unravel the tension around the σ-term is to directly compare with the experimental πN scattering data base. To this end, we compute πN differential cross sections $d\sigma/d\Omega$ using the RS S- and P-wave phase shifts depicted in Fig. 2 as input. For the higher partial waves we use the analysis of [35, 36], with uncertainties estimated following the procedure described in Sect. 2. Some comments are in order. First, at low energy and forward direction, πN cross sections are strongly affected by electromagnetic interactions, which are taken into account following the procedure described in [53]. Second, the discrepancy in the scattering lengths is mainly concentrated in the $I_s = 3/2$ channel: while the KH80 value for the $I_s = 1/2$ channel $a^{1/2}_{0+} = (173 \pm 3.0) \times 10^{-3} M_\pi^{-1}$ is consistent within one standard deviation with the pionic-atom determination in (6), the $I_s = 3/2$ one, $a^{3/2}_{0+} = (-101 \pm 4) \times 10^{-3} M_\pi^{-1}$, lies roughly four standard deviations away. Therefore, it is suggestive to consider the $I_s = 3/2$ channel first, which corresponds to the $\pi^+ p \to \pi^+ p$ reaction. Third, the scattering lengths are used as input inside the RS equations, which, in turn, allow one to generate cross-section solutions in terms of scattering-length values. Fourth, at very low energies, namely for $T_\pi \leq 50\,\text{MeV}$, with $T_\pi = \left(s - (m_N + M_\pi)^2\right)/2m_N$ the kinetic energy of the incoming pion in the lab frame, the scattering lengths used as input dominate the cross section uncertainties. Accordingly, the difference between two different RS cross-section solutions reveals the effect of the scattering lengths used as input. In the same way, one can compare with the experimental data base by defining the χ^2-like function

$$\chi^2_{a^{3/2}_{0+}} = \sum_{i,j} \frac{\left(O^{\text{exp}}_{i,j} - O^{\text{RS}}_{i,j}(a^{3/2}_{0+})\right)^2}{\Delta O^{\text{exp}\,2}_{i,j}}, \tag{12}$$

where $O_{i,j}$ denotes the $\pi^+ p \to \pi^+ p$ differential cross section $d\sigma/d\Omega$, and i, j stand for the incoming pion kinetic energy and the scattering angle, respectively.

The evaluation of the χ^2-like function in (12) with hadronic atom and KH80 scattering lengths provides the results $\chi^2_{\text{HA}}/\text{d.o.f} \approx 0.8$ and $\chi^2_{\text{KH80}}/\text{d.o.f} \approx 4.7$. The corresponding experimental and RS

Table 2. Results for the πN LECs at different orders in the chiral expansion [54].

	NLO	N^{2}LO	N^{3}LO
c_1 [GeV^{-1}]	-0.74 ± 0.02	-1.07 ± 0.02	-1.11 ± 0.03
c_2 [GeV^{-1}]	1.81 ± 0.03	3.20 ± 0.03	3.13 ± 0.03
c_3 [GeV^{-1}]	-3.61 ± 0.05	-5.32 ± 0.05	-5.61 ± 0.06
c_4 [GeV^{-1}]	2.17 ± 0.03	3.56 ± 0.03	4.26 ± 0.04
$\bar{d}_1 + \bar{d}_2$ [GeV^{-2}]	—	1.04 ± 0.06	7.42 ± 0.08
$\bar{d}_3$ [GeV^{-2}]	—	-0.48 ± 0.02	-10.46 ± 0.10
$\bar{d}_5$ [GeV^{-2}]	—	0.14 ± 0.05	0.59 ± 0.05
$\bar{d}_{14} - \bar{d}_{15}$ [GeV^{-2}]	—	-1.90 ± 0.06	
$\bar{e}_{14}$ [GeV^{-3}]	—	—	0.89 ± 0.04
$\bar{e}_{15}$ [GeV^{-3}]	—	—	-0.97 ± 0.06
$\bar{e}_{16}$ [GeV^{-3}]	—	—	-2.61 ± 0.03
$\bar{e}_{17}$ [GeV^{-3}]	—	—	0.01 ± 0.06
$\bar{e}_{18}$ [GeV^{-3}]	—	—	-4.20 ± 0.05

cross section results are plotted in Fig. 4. In view of these results it is clear that only the pionic-atom solution describes the experimental πN data. In addition, since the variation in the scattering lengths is small, RS cross sections are well represented by a linearized version around the pionic-atom scattering length $a^{3/2}_{0+}$. The minimization of (12) using this linearized version of the RS cross section data gives $a^{3/2}_{0+} = -86.6 \times 10^{-3} M_\pi^{-1}$, in perfect agreement with the pionic-atom determination (6).

4 Matching to chiral perturbation theory

The matching to ChPT is one of the most fundamental applications of the RS solution, since it offers a unique opportunity for a systematic determination of πN LECs [54]. One would expect the chiral expansion to work best in a kinematic region where no singularities occur, i.e. where the amplitude can be described solely by a polynomial in the Mandelstam variables. This is precisely the situation encountered in the subthreshold region: the amplitude is purely real, and characterized by its expansion coefficients around ($\nu = 0, t = 0$). The matching is thus most conveniently performed by equating the chiral expansion for the subthreshold parameters to the RS results given in Table 1.

The πN amplitude at N^{3}LO, $\mathcal{O}(p^4)$, involves four NLO LECs, c_i, four (combinations of) N^{2}LO LECs, $\bar{d}_i$, and five N^{3}LO LECs, $\bar{e}_i$, see [55]. These 13 LECs correspond to the 13 subthreshold parameters that receive contributions from LECs in a fourth-order calculation. Inverting the expressions for the subthreshold parameters, we obtain the LECs summarized in Table 2, with correlation coefficients given in [40].

At $\mathcal{O}(p^2)$ only the c_i contribute, and only four subthreshold parameters are sensitive to these LECs. At N^{2}LO four $\bar{d}_i$ appear, and eight subthreshold parameters receive contributions from LECs. Comparing the different extractions up to N^{3}LO, the convergence pattern for the c_i looks reasonably stable. In contrast, while the N^{2}LO $\bar{d}_i$ are of natural size, their values increase by nearly an order of magnitude when going to N LO (except for d_5). The origin of this behavior is due to loop corrections in some subthreshold parameters involving terms that scale with $g_A^2(c_3 - c_4) \sim -16\,\text{GeV}^{-1}$, which are balanced by the large LECs in order to keep the subthreshold parameters at their physical values. Given such large loop corrections the errors for the LECs at a given chiral order are negligible compared to the uncertainties to be attached to the chiral expansion itself. Nevertheless, the enhancement of the c_i can be understood from resonance saturation, which for c_{2-4} is mainly due to the $\Delta(1232)$ [56–58]. In fact, the magnitude of the extracted LECs is sizeably reduced when the Δ is included explicitly in a consistent power counting up to full one-loop order [59] , which, in turn, leads to an improvement of the convergence pattern in the threshold region.

Acknowledgments

We would like to thank the organizers of the XIIth Quark Confinement and the Hadron Spectrum conference in Thessaloniki for a wonderful workshop, and for the invitations to talk about our work on pion–nucleon scattering. Financial support by the Helmholtz Virtual Institute NAVI (VH-VI-417), the DFG (SFB/TR 16, “Subnuclear Structure of Matter”), the Swiss National Science Foundation, and the DOE (Grant No. DE-FG02-00ER41132) is gratefully acknowledged. The work of UGM was also supported by the Chinese Academy of Sciences (CAS) President’s International Fellowship Initiative (PIFI) (Grant No. 2015VMA076).

References

[1] B. Kubis, J. Ruiz de Elvira, M. Hoferichter and U.-G. Meißner, PoS CD **15** (2015) 021.
[2] M. Hoferichter, J. Ruiz de Elvira, B. Kubis and U.-G. Meißner, Phys. Rept. **625** (2016) 1.
[3] S. Weinberg, Phys. Rev. Lett. **17** (1966) 616.
[4] Y. Tomozawa, Nuovo Cim. A **46** (1966) 707.
[5] S. Weinberg, Physica A **96** (1979) 327.
[6] J. Gasser and H. Leutwyler, Annals Phys. **158** (1984) 142.
[7] J. Gasser and H. Leutwyler, Nucl. Phys. B **250** (1985) 465.
[8] M. Hoferichter, B. Kubis, J. Ruiz de Elvira, H.-W. Hammer and U.-G. Meißner, Eur. Phys. J. A **52** (2016) 331.
[9] T. P. Cheng and R. F. Dashen, Phys. Rev. Lett. **26** (1971) 594.
[10] L. S. Brown, W. J. Pardee and R. D. Peccei, Phys. Rev. D **4** (1971) 2801.
[11] A. Bottino, F. Donato, N. Fornengo and S. Scopel, Astropart. Phys. **13** (2000) 215.
[12] J. R. Ellis, K. A. Olive and C. Savage, Phys. Rev. D **77** (2008) 065026.
[13] A. Crivellin, M. Hoferichter and M. Procura, Phys. Rev. D **89** (2014) 054021.
[14] S. M. Roy, Phys. Lett. B **36** (1971) 353.
[15] B. Ananthanarayan, G. Colangelo, J. Gasser and H. Leutwyler, Phys. Rept. **353** (2001) 207.
[16] R. García-Martín, R. Kamiński, J. R. Peláez, J. Ruiz de Elvira, and F. J. Ynduráin, Phys. Rev. D **83** (2011) 074004.
[17] I. Caprini, G. Colangelo and H. Leutwyler, Phys. Rev. Lett. **96** (2006) 132001.
[18] R. García-Martín, R. Kamiński, J. R. Peláez and J. Ruiz de Elvira, Phys. Rev. Lett. **107** (2011) 072001.
[19] G. E. Hite and F. Steiner, Nuovo Cim. A **18** (1973) 237 [CERN-TH-1590 for app. D and E].
[20] J. Stahov, PiN Newslett. **15** (1999) 13.
[21] J. Stahov, PiN Newslett. **16** (2002) 116.

[22] G. E. Hite, W. B. Kaufmann and R. J. Jacob, Phys. Rev. C **71** (2005) 065201.
[23] C. Ditsche, M. Hoferichter, B. Kubis and U.-G. Meißner, JHEP **1206** (2012) 043.
[24] C. Ditsche, M. Hoferichter, B. Kubis and U.-G. Meißner, PoS **CD 12** (2013) 064.
[25] J. Ruiz de Elvira, C. Ditsche, M. Hoferichter, B. Kubis and U.-G. Meißner, EPJ Web Conf. **73** (2014) 05002.
[26] J. Ruiz de Elvira, C. Ditsche, M. Hoferichter, B. Kubis and U.-G. Meißner, Singapore, Singapore: World Scientific (2014) 186.
[27] K. M. Watson, Phys. Rev. **95** (1954) 228.
[28] N. I. Muskhelishvili, *Singular Integral Equations*, Wolters-Noordhoff Publishing, Groningen, 1953 [Dover Publications, 2nd edition, 2008].
[29] R. Omnès, Nuovo Cim. **8** (1958) 316.
[30] M. Hoferichter, C. Ditsche, B. Kubis and U.-G. Meißner, JHEP **1206** (2012) 063.
[31] V. Baru *et al.*, Phys. Lett. B **694** (2011) 473.
[32] V. Baru *et al.*, Nucl. Phys. A **872** (2011) 69.
[33] R. Koch and E. Pietarinen, Nucl. Phys. A **336** (1980) 331.
[34] G. Höhler, *Pion–Nukleon-Streuung: Methoden und Ergebnisse*, in Landolt-Börnstein, **9b2**, ed. H. Schopper, Springer Verlag, Berlin, 1983.
[35] R. A. Arndt, W. J. Briscoe, I. I. Strakovsky and R. L. Workman, Phys. Rev. C **74** (2006) 045205.
[36] R. L. Workman, R. A. Arndt, W. J. Briscoe, M. W. Paris and I. I. Strakovsky, Phys. Rev. C **86** (2012) 035202.
[37] V. Bernard, N. Kaiser and U.-G. Meißner, Phys. Lett. B **389** (1996) 144.
[38] J. Gasser, H. Leutwyler and M. E. Sainio, Phys. Lett. B **253** (1991) 260.
[39] M. Hoferichter, C. Ditsche, B. Kubis and U.-G. Meißner, PoS **CD 12** (2013) 069.
[40] M. Hoferichter, J. Ruiz de Elvira, B. Kubis and U.-G. Meißner, Phys. Rev. Lett. **115** (2015) 092301.
[41] J. Gasser, M. A. Ivanov, E. Lipartia, M. Mojžiš and A. Rusetsky, Eur. Phys. J. C **26** (2002) 13.
[42] M. Hoferichter, B. Kubis and U.-G. Meißner, Phys. Lett. B **678** (2009) 65.
[43] M. Hoferichter, B. Kubis and U.-G. Meißner, Nucl. Phys. A **833** (2010) 18.
[44] J. Gasser, H. Leutwyler and M. E. Sainio, Phys. Lett. B **253** (1991) 252.
[45] S. Dürr *et al.* [BMW Collaboration], Phys. Rev. Lett. **116** (2016) 172001.
[46] Y. B. Yang, A. Alexandru, T. Draper, J. Liang and K. F. Liu [χQCD Collaboration], Phys. Rev. D **94** (2016) 054503.
[47] A. Abdel-Rehim *et al.* [EMT Collaboration], Phys. Rev. Lett. **116** (2016) 252001.
[48] G. S. Bali *et al.* [RQCD Collaboration], Phys. Rev. D **93** (2016) 094504.
[49] M. Hoferichter, J. Ruiz de Elvira, B. Kubis and U.-G. Meißner, Phys. Lett. B **760** (2016) 74.
[50] D. Gotta *et al.*, Lect. Notes Phys. **745** (2008) 165.
[51] T. Strauch *et al.*, Eur. Phys. J. A **47** (2011) 88.
[52] M. Hennebach *et al.*, Eur. Phys. J. A **50** (2014) 190.
[53] B. Tromborg, S. Waldenstrøm and I. Øverbø, Phys. Rev. D **15** (1977) 725.
[54] M. Hoferichter, J. Ruiz de Elvira, B. Kubis and U.-G. Meißner, Phys. Rev. Lett. **115** (2015) 192301
[55] N. Fettes, U.-G. Meißner, M. Mojžiš and S. Steininger, Annals Phys. **283** (2000) 273 [Annals Phys. **288** (2001) 249].
[56] V. Bernard, N. Kaiser and U.-G. Meißner, Int. J. Mod. Phys. E **4** (1995) 193.

[57] V. Bernard, N. Kaiser and U.-G. Meißner, Nucl. Phys. A **615** (1997) 483.
[58] T. Becher and H. Leutwyler, Eur. Phys. J. C **9** (1999) 643.
[59] D. Siemens, J. Ruiz de Elvira, E. Epelbaum, M. Hoferichter, H. Krebs, B. Kubis and U.-G. Meißner, arXiv:1610.08978 [nucl-th].